Multi-faceted investigation: DFT studies and corrosion inhibition potential of 4-(2-((2-methyl-1*H*-indol-3-yl)methylene)hydrazinyl)-phenol for mild steel in 0.5 M HCl medium

A. Jabbar and Y.K. Al-Majedy*

Applied Science Department, University of Technology, P.O. Box 19006, Baghdad, Iraq
**E-mail: YasameenK.Hasan@uotechnology.edu.iq*

Abstract

This research delves into the synthesis, characterization, and corrosion inhibition potential of a novel compound, (*E*)-4-(2-((2-methyl-1*H*-indol-3-yl)methylene)hydrazinyl)phenol, designed to safeguard mild steel against corrosion in a 0.5 M HCl medium. The study emphasizes the complexity of corrosion inhibition, considering factors such as inhibitor properties, surface characteristics, environmental conditions, and adsorption mechanisms. Organic compounds with heightened basicity and electron density on heteroatoms like nitrogen, oxygen, and sulfur demonstrate a proclivity for resisting corrosion. Nitrogen and oxygen, as active sites for adsorption, form protective layers that impede corrosive assaults. This investigation goes beyond synthesis and characterization, introducing a novel dimension by incorporating Density Functional Theory (DFT) studies. The previously unexplored compound, (*E*)-4-(2-((2-methyl-1*H*-indol-3-yl)methylene)hydrazinyl)phenol, undergoes rigorous evaluation as a corrosion inhibitor for mild steel X52 in a 0.5 M HCl medium. DFT studies provide deeper insights into molecular interactions, enhancing the overall understanding of corrosion inhibition. To comprehensively assess corrosion inhibition, electrochemical impedance spectroscopy (EIS) is employed for comparative analysis, shedding light on the compound's potential to mitigate corrosion. By scrutinizing the corrosion inhibition attributes of (*E*)-4-(2-((2-methyl-1*H*-indol-3-yl)methylene)hydrazinyl)phenol, this research advances the understanding of corrosion mechanisms and introduces a promising contender in the domain of corrosion-resistant materials. As industries increasingly seek eco-friendly processes and sustainable solutions, exploring this derivative underscores its potential contribution to corrosion inhibition, providing valuable insights for future industrial applications. This multifaceted approach, encompassing synthesis, characterization, electrochemical analysis, and DFT studies, represents a significant stride toward a comprehensive understanding of corrosion inhibition mechanisms and the development of effective corrosion protection strategies, including weight loss methods as part of the assessment.

Received: November 27, 2023. Published April 29, 2024 doi: 10.17675/2305-6894-2024-13-2-8

Keywords: *anti-corrosion, 2-methylindole-3-carboxaldehyde, mild steel, inhibition efficiency.*

1. Introduction

Mild steel, renowned for its versatility in applications spanning structural, industrial, instrumental, and automotive realms, confronts a persistent adversary: corrosion [1–3]. The repercussions of this challenge are profound, manifesting in economic losses due to repairs, replacements, and diminished product integrity. Industries such as acid cleaning, pickling, descaling, and oil and gas exploration, where acidic environments are prevalent, are particularly vulnerable to the corrosive degradation of iron and steel surfaces [4–7]. In response, corrosion inhibition strategies have emerged as pivotal defense mechanisms. These strategies involve the introduction of corrosion inhibitors, compounds that effectively temper the corrosion process within corrosive environments, without significantly altering the concentration of corrosive agents [8–11]. Mild steel, a vital engineering material across diverse sectors, confronts corrosion challenges, particularly in acidic environments prevalent in industries such as acid cleaning, pickling, descaling, and oil and gas exploration. In response to these challenges, effective corrosion mitigation strategies are imperative. Corrosion inhibitors, whether derived naturally or synthesized, play a pivotal role in mitigating corrosion without significantly altering the concentration of corrosive agents. The mechanisms of corrosion inhibition are intricate, involving the modulation of cathodic and anodic reactions to redirect or stabilize the metal's corrosion potential. The intricacies of corrosion inhibition encompass modulation of cathodic and anodic reactions, influencing the corrosion potential of metals to thwart the deterioration process. The effectiveness of corrosion inhibitors is rooted in their intrinsic properties, including the affinity of organic compounds for heteroatoms such as nitrogen, oxygen, and sulfur, which imbue them with a propensity to resist corrosion [12–15]. Such compounds interact with metal surfaces, forming protective layers that mitigate the corrosive impact. In this study, we focus on a novel corrosion inhibitor, namely "(*E*)-4-(2-((2-methyl-1*H*-indol-3-yl)methylene)-hydrazinyl)phenol". This inhibitor is distinguished by its nitrogen-containing heteroaromatic structure. Despite its uncharted territory in corrosion inhibition, it holds promise as a potential safeguard against the corrosive degradation of mild steel X52 within a 0.5 M HCl medium [16]. Through the integration of electrochemical impedance spectroscopy (EIS) and Density Functional Theory (DFT) studies, this research pursues a multifaceted exploration of the corrosion inhibition capabilities of (*E*)-4-(2-((2-methyl-1*H*-indol-3-yl)methylene)-hydrazinyl)phenol (Figure 1). By unraveling the corrosion inhibition potential of this novel inhibitor, we aim to fill critical gaps in our comprehension of corrosion mechanisms and, concurrently, open a pioneering pathway for enhanced corrosion protection strategies. This multifaceted approach, encompassing experimental analysis through EIS, weight loss methods and molecular insights via DFT [17] studies, not only expands our understanding of the molecular interactions between the inhibitor and the mild steel surface but also introduces a new dimension to the realm of corrosion-resistant materials. In a world where industries are increasingly inclined toward sustainable and eco-friendly practices,

investigating the efficacy of this inhibitor holds the promise of offering valuable insights that resonate across a spectrum of industrial applications [18].

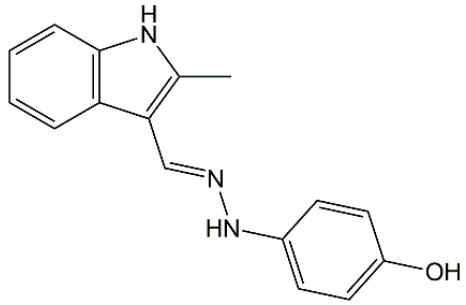

Figure 1. Chemical structure of (*E*)-4-(2-((2-methyl-1*H*-indol-3-yl)methylene)hydrazinyl)phenol.

2. Materials and Methods

2.1. Specimen preparation

Mild steel X52 specimens, chemically composed of 0.16% carbon, 0.45% silicon, 1.65% manganese, 0.02% phosphorus, 0.01% sulphur, 0.07% vanadium, 0.05% niobium, 0.04% titanium, with iron constituting the remainder, were employed in this study. To prepare the specimens for experimentation, surfaces were polished to ensure uniformity and cleanliness. The surface area of each specimen was meticulously determined before subjecting them to various tests.

2.2. Synthesis of (E)-4-(2-((2-methyl-1H-indol-3-yl)methylene)hydrazinyl)phenol

The synthesis of (*E*)-4-(2-((2-methyl-1*H*-indol-3-yl)methylene)hydrazinyl)phenol involved several steps. First, ethyl-4-hydroxybenzoate was prepared by refluxing 4-hydroxycarboxylic acid (30 g, 2.245 moles) with absolute ethanol and concentrated sulfuric acid (2.5 ml, 2.245 moles) for four hours. Next, 4-hydroxybenzoylhydrazide was synthesized by refluxing a mixture of ethyl-4-hydroxybenzoate (10 ml, 0.069 moles) and hydrazine hydrate (0.069 moles) in 50 ml of pure ethanol for an hour. The resulting mixture was filtered after ethanol was added. In the final step, 4-(2-((2-methyl-1*H*-indol-3-yl)methylene)hydrazinyl)phenol was synthesized by refluxing 4-hydroxybenzoylhydrazide with 2-methylindole-3-carboxaldehyde in glacial acetic acid (5 drops) and 100% ethanol, creating a Schiff base, followed by a 10-hour reflux. The product (Figure 2) was filtered and recrystallized using ethanol.

2.3. Solutions

The corrosive environment of 0.5 M hydrochloric acid required for corrosion inhibition tests was prepared by adding 37% analytical grade hydrochloric acid (HCl) to deionized water. Corrosion inhibitor solutions were prepared by dissolving the inhibitor in 1.0 mM concentrations [19–22].

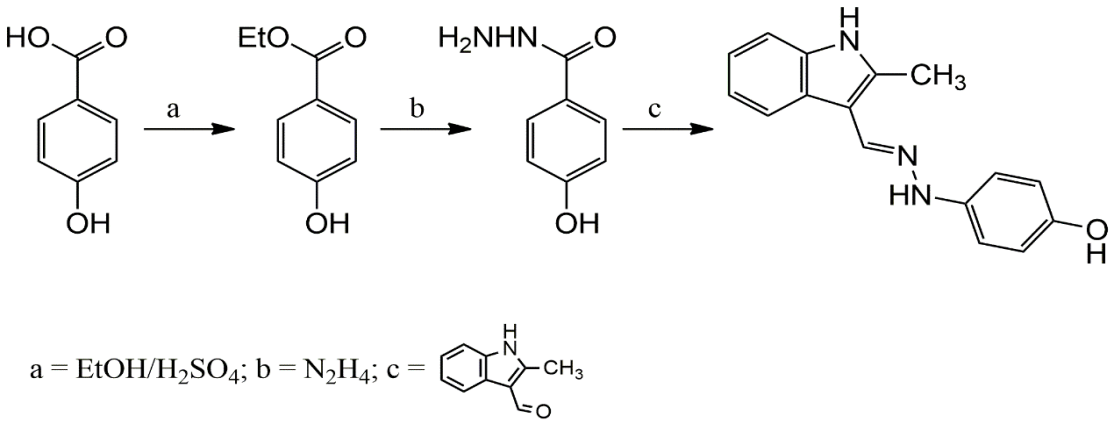

Figure 2. The synthesis of the corrosion inhibitor.

2.4. Electrochemical studies

Open circuit potential (OCP): Open circuit potential measurements were conducted in a 0.6 N acidic electrolyte prior to the electrochemical measurements. The specimens were immersed in the electrolyte for 15 minutes, followed by measuring the open circuit potential for 30 minutes. Tafel graph measurements: Tafel measurements for carbon steel specimens were performed using the potentiodynamic mode in the electrolyte. A conventional three-electrode cell setup was used, with a saturated calomel electrode (SCE) as the reference electrode, a platinum plate as the counter electrode, and the specimens as the working electrode. Polarization was achieved by scanning the initial potential from the negative value to the previously measured OCP, with the final potential being positive. The potential range was from −250 mV to +250 mV *versus* OCP, with a scan rate of 1 mV/s. The electrochemical studies were conducted using the CS 310 CorrTest workstation, Wuhan, China.

2.5. Weight loss techniques

1. **Sample preparation:** Mild steel X52 specimens were mechanically polished using successive grades of emery paper up to 1200 grit, followed by ultrasonic cleaning in acetone to ensure a clean and uniform surface. The specimens were then air-dried prior to the immersion experiments.
2. **Inhibitor synthesis and concentration preparation:** The corrosion inhibitor, (*E*)-4-(2-((2-methyl-1*H*-indol-3-yl)methylene)hydrazinyl)phenol, was synthesized by the previously established procedure. Various inhibitor concentrations were prepared by diluting the synthesized compound in the 0.5 M HCl medium, resulting in concentrations of 0.10×10^{-2}, 15×10^{-2}, 20×10^{-2}, 25×10^{-2}, and 50×10^{-2} M.
3. **Immersion experiments:** The mild steel X52 specimens were immersed in the prepared 0.5 M HCl solutions with different inhibitor concentrations for distinct time periods of 1 hour, 3 hours, 24 hours, 48 hours, and 72 hours. For each time period and inhibitor concentration, triplicate specimens were used to ensure reliability and reproducibility of the results.

4. **Weight loss measurements:** After each immersion time, the mild steel specimens were carefully removed from the solution, rinsed with distilled water, and dried. The weight loss due to corrosion was determined by measuring the weight difference between the initial and final states of each specimen using a high-precision analytical balance.
5. **Data analysis:** The corrosion rates were calculated using the weight loss measurements and the corresponding surface areas of the mild steel specimens. The influence of the inhibitor concentrations on the corrosion inhibition efficiency was assessed by comparing the corrosion rates at each immersion time period. Statistical analysis was performed to validate the significance of the results.
6. **Control experiments:** Control experiments were conducted using the 0.5 M HCl solution without the corrosion inhibitor to establish baseline corrosion rates for comparison with the inhibited systems.
7. **Instrumentation:** All experimental procedures were carried out in accordance with safety guidelines. The analytical balance used for weight measurements was calibrated regularly, and the inhibitor concentrations were verified through analytical techniques such as UV-Vis spectroscopy.
8. **Reproducibility:** To ensure the reproducibility of the weight loss measurements, the immersion experiments were repeated and the results were found to be consistent within acceptable experimental error limits.

The corrosion rate (C_R) and inhibition efficiency *IE*% can be calculated using the weight loss method with the following equations (1 and 2):

$$C_R = \frac{WL}{S \times t} \tag{1}$$

$$IE\% = \left(1 - \frac{C_{R(inh)}}{C_{R(uninh)}}\right) \times 100 \tag{2}$$

where: *WL* is the mass loss of the specimen due to corrosion (in grams); *S* is the surface area of the specimen exposed to the corrosive medium (cm^2); *t* is the time duration of immersion in the corrosive medium (in hours); $C_{R(inh)}$ and $C_{R(uninh)}$ is the corrosion rate in the presence and in the absence of the inhibitor, respectively.

This equation expresses the percentage reduction in corrosion rate achieved by the corrosion inhibitor compared to the uninhibited system. Higher inhibition efficiency indicates a more effective corrosion inhibition performance of the tested compound.

2.6. Surface analysis

The surface of the mild steel specimens was analysed using a field emission scanning electron microscope (FESEM). FESEM images were captured after immersing the samples in the test solution for 2 hours at 25°C, both in the absence and presence of 7.5 mM of the inhibitors.

2.7. Density Functional Theory (DFT) studies

To gain a deeper understanding of the molecular interactions between the synthesized inhibitor, "(*E*)-4-(2-((2-methyl-1*H*-indol-3-yl)methylene)hydrazinyl)phenol", and the mild steel surface, Density Functional Theory (DFT) calculations were performed. DFT is a powerful computational tool widely used in materials science and chemistry to elucidate the electronic structure, energetics, and thermodynamic properties of molecular systems. DFT calculations were carried out using state-of-the-art quantum chemistry software. The initial geometry of the inhibitor molecule was optimized using a suitable level of theory and basis set, B3LYP/6-31G (d). The mild steel surface model was constructed to mimic the relevant adsorption sites, and its geometry was optimized in the presence of the inhibitor. Molecular orbital analysis was conducted to investigate the electronic structure of the inhibitor-mild steel complex. The distribution of frontier molecular orbitals, such as Highest Occupied Molecular Orbital (HOMO) and Lowest Unoccupied Molecular Orbital (LUMO), provides insights into the electron transfer processes involved in the adsorption mechanism [23].

3. Results and Discussion

3.1. Chemistry

The characteristics of the compounds synthesized are outlined below:

a. **Ethyl 2-chlorobenzoate:** The synthesis of ethyl-2-chlorobenzoate resulted in a melting point of 143–147°C, yielding 55%. The molecular weight was determined as 156.5 g/mol. Fourier Transform Infrared Spectroscopy (FT-IR) analysis displayed characteristic peaks at 570–858 cm^{-1} (C–Cl stretching), 1313–1406 cm^{-1} (CH_2, CH_3 bending), 1585 cm^{-1} (C=C stretching), 1689 cm^{-1} (C=O stretching), and 3091 cm^{-1} (CH stretching). Nuclear Magnetic Resonance (NMR) analysis revealed peaks at 1.29 ppm (triplet, 3H, CH_3), 4.30 ppm (quartet, 2H, CH_2), and 7.44–7.99 ppm (multiple, 4H, aromatic ring).

b. **Ethyl 4-hydroxybenzoate:** The synthesis of ethyl-4-hydroxybenzoate yielded a melting point of 114–119°C with a 55% yield. The molecular weight was determined as 138.12 g/mol. FT-IR analysis exhibited peaks at 1288 cm^{-1} (C–O stretching), 1373–1448 cm^{-1} (CH_2, CH_3 bending), 1516–1600 cm^{-1} (C=C stretching), 1674 cm^{-1} (C=O stretching), 2978 cm^{-1} (CH stretching), and 3223 cm^{-1} (OH stretching). NMR analysis showed peaks at 1.29 ppm (triplet, 3H, CH_3), 4.30 ppm (quartet, 2H, CH_2), 5.35 ppm (singlet, 1H, OH), and 6.81–7.88 ppm (doublet-doublet, 4H, aromatic ring).

c. **4-Hydroxybenzohydrazide:** The synthesis of 4-hydroxybenzohydrazide resulted in a melting point of 120–125°C with a 60% yield. The molecular weight was determined as 128 g/mol. FT-IR analysis revealed peaks at 1597 cm^{-1} (C=C stretching), 1647 cm^{-1} (NH–C=O bending), 3057 cm^{-1} (OH stretching), 3184 cm^{-1} (NH stretching), and 3286 cm^{-1} (NH_2 stretching). NMR analysis displayed peaks at

2.0 ppm (singlet, 2H, NH_2), 5.35 ppm (singlet, 1H, OH), 6.88–7.86 ppm (doublet-doublet, 4H, aromatic ring), and 8.0 ppm (singlet, 1H, NH).

d.4-(2-((2-Methyl-1*H*-indol-3-yl)methylene)hydrazinyl)phenol: The synthesis of 4-(2-((2-methyl-1*H*-indol-3-yl)methylene)hydrazinyl)phenol yielded a melting point of 107–111°C with a 65% yield. The molecular weight was determined as 293 g/mol. FT-IR analysis displayed peaks at 1460 cm^{-1} (CH_3 bending), 1608 cm^{-1} (C=C stretching), 1641 cm^{-1} (NH–C=O bending), 1680 cm^{-1} (C=N stretching), 2922–2980 cm^{-1} (C–H stretching), 3061 cm^{-1} (C–H aromatic stretching), 3221 cm^{-1} (NH stretching), and 3221 cm^{-1} (OH stretching). NMR analysis revealed peaks at 1.29 ppm (singlet, 3H, CH_3), 4.26 ppm (singlet, 1H, OH), 6.80–7.80 ppm (multiplet, 8H, aromatic ring), 7.0 ppm (singlet, 1H, NH–N), 8.90 ppm (singlet, 1H, CH=N), and 11.43 ppm (singlet, 1H, NH indole).

The results of the chemical analyses confirm the successful synthesis of the compounds and provide insights into their structural characteristics. These synthesized compounds serve as the foundation for subsequent corrosion inhibition studies.

3.2. Electrochemical tests

Polarization measurements were conducted to glean insights into the anodic and cathodic kinetics involved in the corrosion process. The electrochemical kinetic parameters encompassing corrosion current, Tafel slopes (b_a and b_c), corrosion potential (E_{corr}), and corrosion rate (C_R) were derived from the polarization curves. The data extracted from these measurements are summarized in Table 1. Inhibition efficiency (*IE*) and surface coverage (θ) can be quantified using Equations 3 and 4, respectively [24, 25]:

Inhibition efficiency (%):
$$IE = \frac{C_R - C_{Ri}}{C_R} \times 100 \quad (3)$$

Surface coverage (θ):
$$\theta = \frac{C_R - C_{Ri}}{C_R} \quad (4)$$

where C_R represents the corrosion rate in the absence of the tested inhibitor, and C_{Ri} represents the corrosion rate in the presence of the tested inhibitor.

As observed from Table 2, the introduction of the corrosion inhibitor leads to a shift in the corrosion potential (E_{corr}) towards more negative values. This shift signifies the formation of a protective layer on the mild steel coupons' surface, which adsorbs the inhibitor molecules produced in the solution. Furthermore, the reduction in anodic and cathodic current densities facilitates the adsorption of the inhibitor molecules onto the mild steel surface, accelerating the process. Figures 3 and 4 along with Tables 1 and 2 illustrate the potential polarization curve for mild steel in a hydrochloric acid solution both in the absence and presence of inhibitor molecules. The presence of inhibitors correlates with diminished values of current density (i_{corr}) and corrosion rate (C_R), indicating enhanced inhibition efficiency. In essence, the dissolution of the anodic metal and the cathodic reactions

responsible for hydrogen gas production are significantly impeded. The inhibitor addition to the acid medium affects both the anodic and cathodic segments of the Tafel slopes [26–28].

Table 1. Corrosion rate, surface coverage, and inhibitor efficiency.

Compounds	C_R (mg/cm²·hr)	Surface coverage	*IE* (%)
Blank	0.888	–	–
1 mM	0.292	0.671	67.1

Table 2. Polarization data for mild steel in 0.5 M HCl without and with inhibitor at 25°C.

Concentrations	E_{corr} (V)	i_{corr} (A/cm²)	b_c (mV)	b_a (mV)	C_R (mm/a)	θ	*IE* (%)
0 mM	–0.469	7.575	101.19	74.747	0.888	–	–
1 mM	–0.448	2.495	110.35	72.264	0.292	0.671	67.1

The polarization data encapsulated in these tables underscore the protective effect of the inhibitors on mild steel corrosion within a hydrochloric acid environment. The shift in potential, reduction in current densities, and subsequent decrease in corrosion rate collectively affirm the efficiency of these inhibitors in attenuating the corrosive processes, thereby enhancing the durability of mild steel in aggressive conditions [29–34].

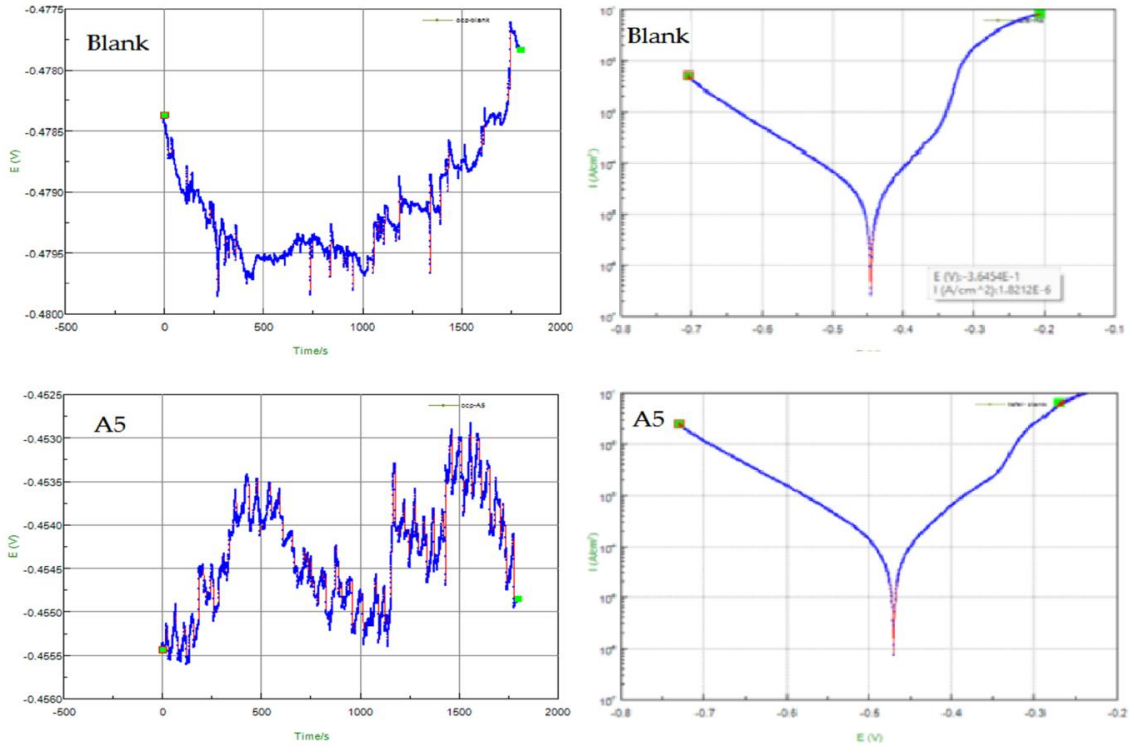

Figure 3. The potential polarization curve for mild steel in a hydrochloric acid solution both in the absence and presence of inhibitor molecules.

3.3. Weight loss techniques and corrosion inhibition performance

The corrosion inhibition efficiency (*IE*) of the synthesized compound, (*E*)-4-(2-((2-methyl-1*H*-indol-3-yl)methylene)hydrazinyl)phenol, in a 0.5 M HCl medium was assessed through weight loss measurements at various immersion time periods and inhibitor concentrations[35].

The results are presented in Table 1, where *IE* is expressed as a percentage for each concentration of the compound at 1 hr, 3 hr, 24 hr, 48 hr, and 72 hr immersion times.

3.3.1. Effect of inhibitor concentration:

The corrosion inhibition efficiency is notably influenced by the concentration of the inhibitor. As depicted in Table 3 and Figure 4, an increase in the concentration of compound (1) correlates with a general enhancement in *IE*. For instance, at the 1 hr immersion time, *IE* gradually increases from 15% at 0×10^{-2} mM to 34% at 50×10^{-2} mM. This trend is consistent across all the investigated immersion periods, indicating a concentration-dependent inhibition effect.

3.3.2. Variation with immersion time:

The impact of immersion time on the corrosion inhibition performance is evident from the table. As the immersion time extends, the *IE* values tend to rise, reaching their peak at 72 hr. For instance, at the highest concentration of 50×10^{-2} mM, *IE* progresses from 30% at 1 hr to 75% at 72 hr. This suggests that the compound's inhibitive action becomes more pronounced with prolonged exposure to the corrosive environment.

3.3.3. Optimal inhibitor performance:

The optimal inhibitor performance is observed at 72 hr immersion time, with the highest *IE* of 75% achieved at a concentration of 50×10^{-2} mM. This underscores the compound's potential for providing sustained and effective corrosion protection over an extended period.

3.3.4. Comparative analysis:

Comparative analysis of *IE* values at different concentrations and time intervals allows for the identification of the most effective conditions for corrosion inhibition. The compound exhibits promising corrosion inhibition potential, with *IE* values reaching 75% under specific conditions. In summary, the weight loss techniques employed in this study reveal a concentration-dependent and time-sensitive corrosion inhibition performance of the synthesized compound. These findings contribute valuable insights into the compound's effectiveness as a corrosion inhibitor and provide a basis for optimizing its application in practical industrial settings. Further analysis and experimentation are warranted to fully understand the underlying mechanisms governing the observed corrosion inhibition trends.

Table 3. Inhibitor efficiency (*IE*%) of compound (1) in 0.5 M HCl.

Concentration of compound (1)	%*IE* at				
	1 hr	**3 hr**	**24 hr**	**48 hr**	**72 hr**
0×10^{-2} mM	0	0	0	0	0
10×10^{-2} mM	15	25	30	35	40
15×10^{-2} mM	20	30	35	40	45
20×10^{-2} mM	25	35	40	45	50
25×10^{-2} mM	30	40	45	56	65
50×10^{-2} mM	34	45	55	60	75

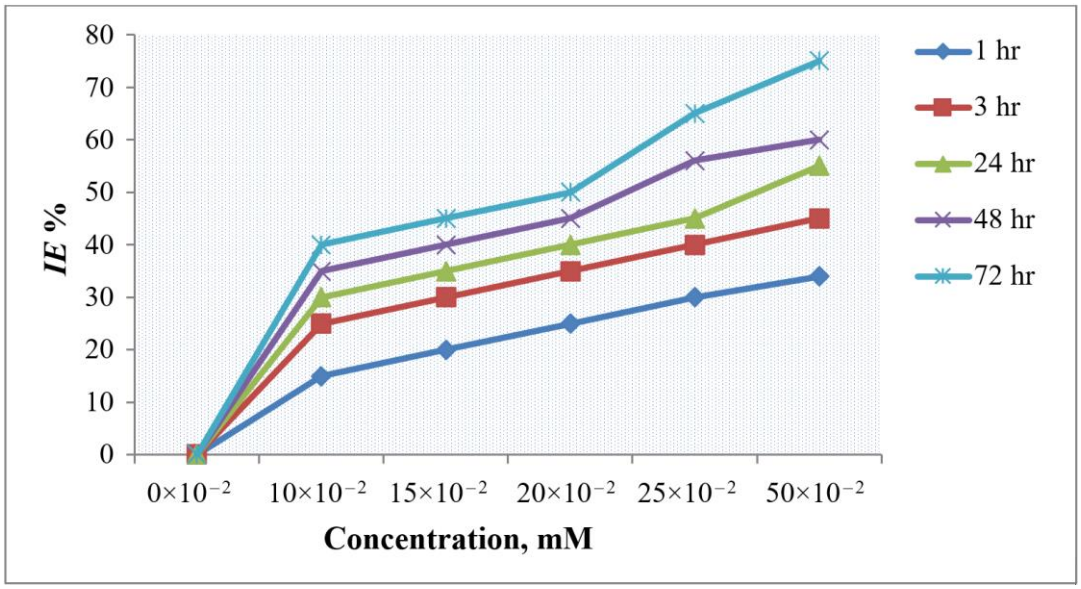

Figure 4. The effect of inhibition efficiency against corrosion for different immersion periods.

3.4. Temperature-dependent corrosion inhibition performance

The corrosion inhibition efficiency (*IE*) of the synthesized compound, (*E*)-4-(2-((2-methyl-1*H*-indol-3-yl)methylene)hydrazinyl)phenol, in a 0.5 M HCl medium was investigated at various temperatures, as presented in Table 4 and depicted graphically in Figure 5. The *IE* values are expressed as a percentage for each concentration of the compound at temperatures of 308 K, 313 K, 323 K, 333 K, and 343 K.

1. Temperature influence on corrosion inhibition: As evident from Table 4 and Figure 5, temperature plays a significant role in the corrosion inhibition performance of the compound. Generally, an increase in temperature leads to a reduction in *IE* values at each concentration of the inhibitor. For instance, at 0×10^{-2} mM, the *IE* decreases from 35% at 308 K to 27% at 343 K.

2. Optimal inhibition efficiency: The data suggest that the optimal inhibition efficiency is observed at lower temperatures. At 308 K, the compound exhibits the highest *IE* values, reaching 53% at the highest concentration of 50×10^{-2} mM. This implies that the inhibitor is more effective in mitigating corrosion at lower temperatures.
3. Temperature-dependent trends: A consistent trend is observed across concentrations, where *IE* values tend to decrease with increasing temperature. This indicates that the inhibitive action of the compound is more pronounced at lower temperatures, and its effectiveness diminishes as the temperature rises.
4. Practical implications: Understanding the temperature dependence of the inhibitor is crucial for practical applications, especially in industries where variations in temperature are common. The compound may be particularly well-suited for scenarios involving lower operating temperatures, where it can provide robust corrosion protection.
5. Correlation with environmental conditions: The observed temperature-dependent trends underscore the importance of considering environmental conditions when assessing the performance of corrosion inhibitors. Factors such as seasonal changes or specific industrial processes that involve temperature fluctuations should be taken into account for effective inhibitor application.

In conclusion, the temperature-dependent corrosion inhibition performance of compound (1) is evident from the experimental data. Lower temperatures favor higher inhibition efficiency, highlighting the need for a nuanced understanding of the compound's behaviour under different temperature conditions. This knowledge contributes to the strategic deployment of the inhibitor in real-world applications, enhancing its effectiveness in diverse operational environments. Further investigations into the underlying mechanisms governing the temperature sensitivity of the inhibitor would be valuable for a comprehensive understanding of its performance.

Table 4. Inhibitor efficiency %*IE* of compound (1) in 0.5 M HCl.

Concentration of compound (1)	**%*IE* at**				
	308 K	**313 K**	**323 K**	**333 K**	**343 K**
0×10^{-2} mM	0	0	0	0	0
10×10^{-2} mM	35	33	31	29	27
15×10^{-2} mM	39	37	35	31	26
20×10^{-2} mM	42	40	38	33	28
25×10^{-2} mM	49	45	41.3	35	30.1
50×10^{-2} mM	53	51	45.6	37	33

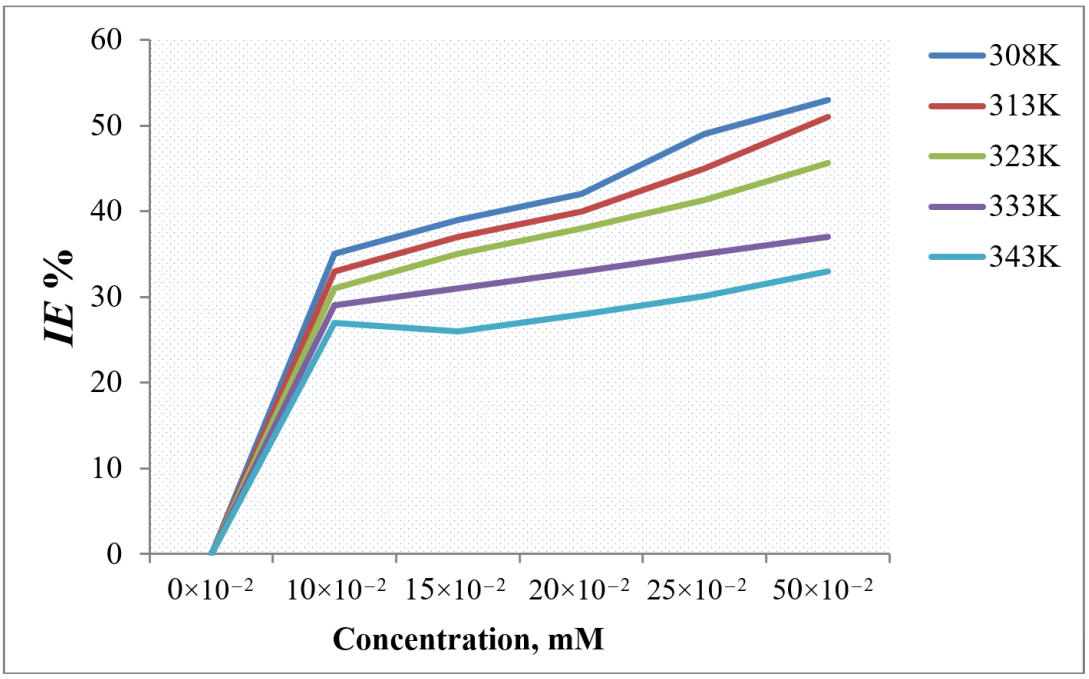

Figure 5. The effect of inhibition efficiency against corrosion for different temperatures.

3.5. Mechanism of inhibition: understanding the adsorption process

The mechanism underlying the inhibition of mild steel corrosion in a 0.5 M HCl medium by the synthesized compound involves the intricate adsorption of inhibitor molecules at the interface between the mild steel and the corrosive solution. This adsorption phenomenon is driven by a combination of physical and chemical interactions, where the nature of the alloy, inhibitor molecules, electrolyte composition, temperature, and specimen structure all play crucial roles in shaping the inhibition process [36]. In the context of organic inhibitors, their modes of interaction with the mild steel surface encompass physical adsorption, chemical adsorption, or a synergistic combination of both. Central to these interactions is the electronic density, a key parameter that dictates the probability of electron presence, at specific functional sites within the inhibitor molecule [37]. This electronic density determines the efficacy of inhibition, as higher electronic densities enhance the likelihood of effective adsorption and subsequent protective film formation [37–42].

Thermodynamic insights gleaned from the adsorption process reveal a dual nature, wherein both chemical and physical adsorptions coexist during the interaction between the inhibitor molecules and the mild steel surface within the 0.5 M HCl environment [43–45]. The chemisorption, or chemical adsorption, of inhibitor molecules onto the mild steel surface can be attributed to a variety of intricate interactions. Notably, the pyrrole and benzene rings within the inhibitor molecule establish interactions with the unoccupied d-orbitals of iron atoms residing on the mild steel surface. Additionally, the unshared electron pairs of heteroatoms, particularly nitrogen and oxygen, participate in bonding with the metal surface (Figure 6). The resonance-rich π-electron systems of the azomethine groups within the inhibitor further contribute to the chemisorption process [46–50]. The orchestration of these

interactions results in the formation of a protective layer or film on the mild steel surface. This layer acts as a barrier, effectively shielding the metal from the corrosive attack of the surrounding acidic medium. Through a delicate interplay of physical and chemical forces, the inhibitor molecules establish a robust connection with the metal surface, thereby mitigating the corrosion process. The combined effects of chemisorption, physical adsorption, and the formation of this protective barrier collectively contribute to the observed reduction in corrosion rates and enhanced inhibition efficiency in the presence of the synthesized inhibitor. In summary, the mechanism of inhibition in this context involves a multifaceted process of adsorption, where the inhibitor molecules interact with the mild steel surface through both chemical and physical routes. This intricate interplay underscores the potential of the synthesized compound as an effective corrosion inhibitor, offering new avenues for the development of advanced corrosion protection strategies [51].

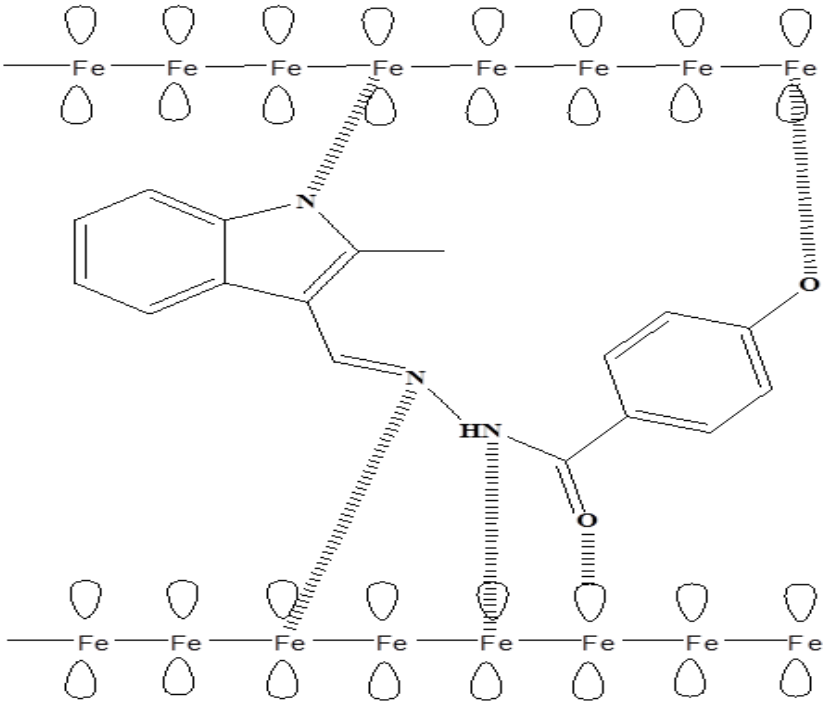

Figure 6. The suggested mechanism of inhibitor molecules.

3.6. Surface analysis: Insights from microscopy

3.6.1. FESEM imaging: Unveiling surface transformations

Figure 7a and 7b present striking field emission scanning electron microscope (FESEM) images capturing the evolution of the mild steel surface. The first image, Figure 7a, depicts the polished surface of the mild steel specimen prior to immersion in the test solution. As we examine the second image, Figure 7b, it becomes evident that the surface morphology undergoes a dramatic transformation after immersion in the aggressive environment of the 1 M HCl solution for 2 hours. The surface is now marked by roughness and extensive corrosion damage, a direct consequence of the corrosive acid attack.

3.6.2. The significance of protective layers

These FESEM images not only provide a tangible visualization of the corrosion protection offered by the synthesized inhibitors but also offer a visual understanding of the mechanism underlying their efficiency. The formation of a protective layer, visible as a smooth surface, effectively prevents the penetration of the corrosive ions into the mild steel matrix. This layer, a result of intricate interactions between the inhibitor molecules and the metal surface, ensures the durability and longevity of the mild steel, even in the challenging environment of an acidic medium. In summary, the FESEM images showcased in Figure 7 underscore the critical role of the synthesized inhibitors in transforming the mild steel surface from a state of susceptibility to corrosion to a state of enhanced resistance. The formation of a protective layer is a tangible manifestation of the inhibitors' ability to safeguard the metal against the harsh conditions of the acidic environment, presenting a promising avenue for effective corrosion protection strategies.

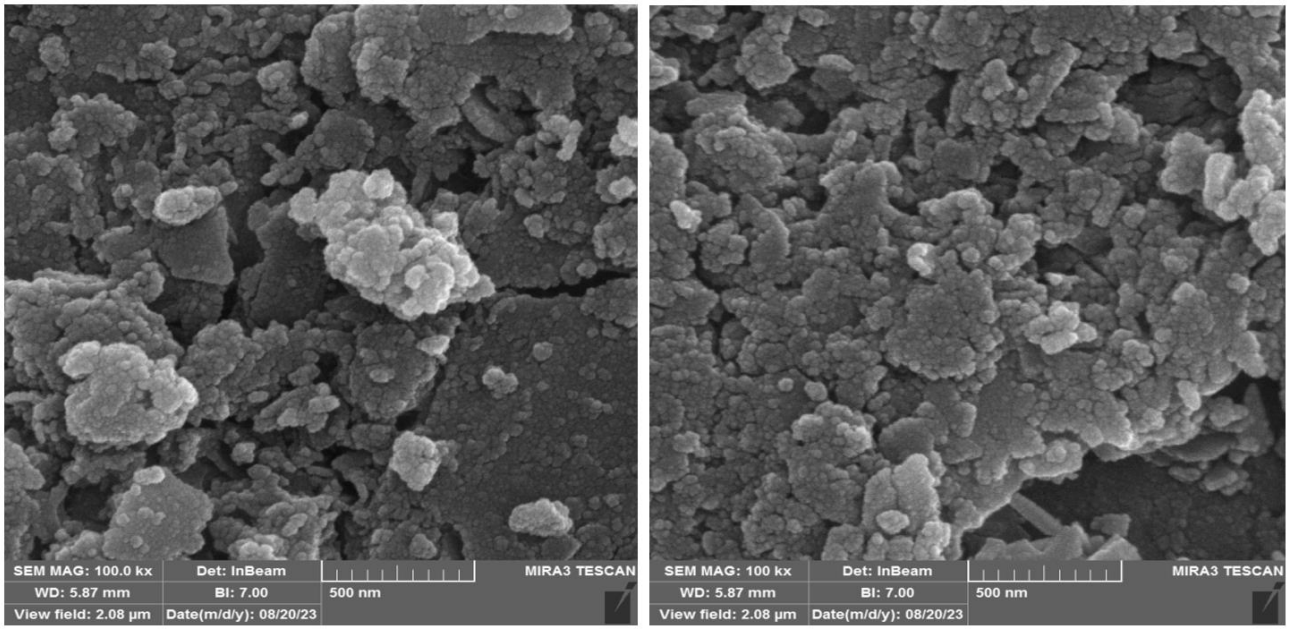

(a) (b)

Figure 7. FESEM images of mild steel surface: (a) immersed in 0.5 M HCl for 2 h, (b) immersed in 0.5 M HCl with inhibitor for 2 h.

3.7. DFT

The calculated electronegativity of the inhibitor molecule as in Table 5 is approximately –4.8575 eV. Electronegativity represents the tendency of an atom or molecule to attract electrons. A lower electronegativity indicates a reduced ability to attract electrons compared to the iron atom (χ_{iron}=7 eV). The calculated hardness of the inhibitor molecule is approximately 3.7525 eV. Hardness reflects the resistance of a system to electron flow or charge transfer. A higher hardness value suggests a more stable and less reactive system. In

this case, the inhibitor exhibits relatively high hardness compared to the iron atom (η_{iron}=0 eV), indicating a greater stability of the inhibitor. Calculated softness of the inhibitor molecule is approximately 0.1333 eV^{-1}. Softness is the reciprocal of hardness and provides insights into the system's reactivity. A lower softness value indicates a less reactive system. In this context, the inhibitor's low softness implies a reduced tendency for reactivity, making it suitable for inhibiting corrosion. The inhibitor molecule exhibits a ΔN value of approximately –2.8575 eV. This value represents the difference in electronegativity between the inhibitor and iron. Negative ΔN values suggest that electrons are transferred from the inhibitor to iron during the adsorption process. This electron transfer contributes to the formation of a protective layer on the mild steel surface. These results collectively suggest that the inhibitor molecule, with its relatively low electronegativity, high hardness, low softness, and negative ΔN value, possesses attributes conducive to effective corrosion inhibition. The calculated parameters indicate that the inhibitor is likely to form stable adsorption configurations on the mild steel surface, reducing the susceptibility of the metal to corrosion in the acidic environment. Further experimental validation and analysis can confirm the inhibitor's potential as an effective corrosion inhibitor for mild steel in 0.5 M HCl medium.

Table 5. The quantum chemical parameters for the synthesized inhibitor.

Parameter	Formula	Value (eV)
Electronegativity (χ)	$\chi=-(HOMO+LUMO)/2$	–4.8575 eV
Hardness (η)	$\eta=(HOMO-LUMO)/2$	3.7525 eV
Softness (S)	$S=1/(2\cdot\eta)$	0.1333 eV^{-1}
Fractional number of electrons transferred (ΔN)	$\Delta N=\chi-\chi_{iron}$	–2.8575 eV
Iron's electronegativity (χ_{iron})	χ_{iron}=7 eV	7 eV
Iron's hardness (η_{iron})	η_{iron}=0 eV	0 eV

Figure 8 showcases the molecular structure of the inhibitor, (*E*)-4-(2-((2-methyl-1*H*-indol-3-yl)methylene)hydrazinyl)phenol, along with its Highest Occupied Molecular Orbital (HOMO) and Lowest Unoccupied Molecular Orbital (LUMO) structures. This representation provides valuable insights into the electronic properties and reactivity of the inhibitor.

- Molecular Structure: The molecular structure of the inhibitor reveals its chemical composition and arrangement of atoms. It highlights the key functional groups and structural features that contribute to its corrosion inhibition potential. The presence of nitrogen and oxygen heteroatoms suggests potential sites for interaction with the mild steel surface.

- HOMO Orbital: The HOMO orbital represents the highest energy level in which electrons are found in the inhibitor molecule. In Figure 8, the HOMO orbital is depicted, illustrating the electron density distribution within the molecular framework. Regions of high electron density in the HOMO orbital are indicative of areas where electrons are most likely to be donated during chemical interactions.
- LUMO Orbital: In contrast, the LUMO orbital represents the lowest unoccupied energy level, signifying regions where electrons can be accepted. The LUMO orbital, as shown in Figure 8, provides insights into the regions where the inhibitor can potentially accept electrons or participate in electron transfer processes.

The Figure 8 collectively presents a comprehensive overview of the inhibitor's structural and electronic characteristics, offering a foundation for understanding its interactions with the mild steel surface in the context of corrosion inhibition. These visual representations are invaluable for elucidating the mechanisms underlying the inhibitor's effectiveness in protecting mild steel from corrosion in acidic environments.

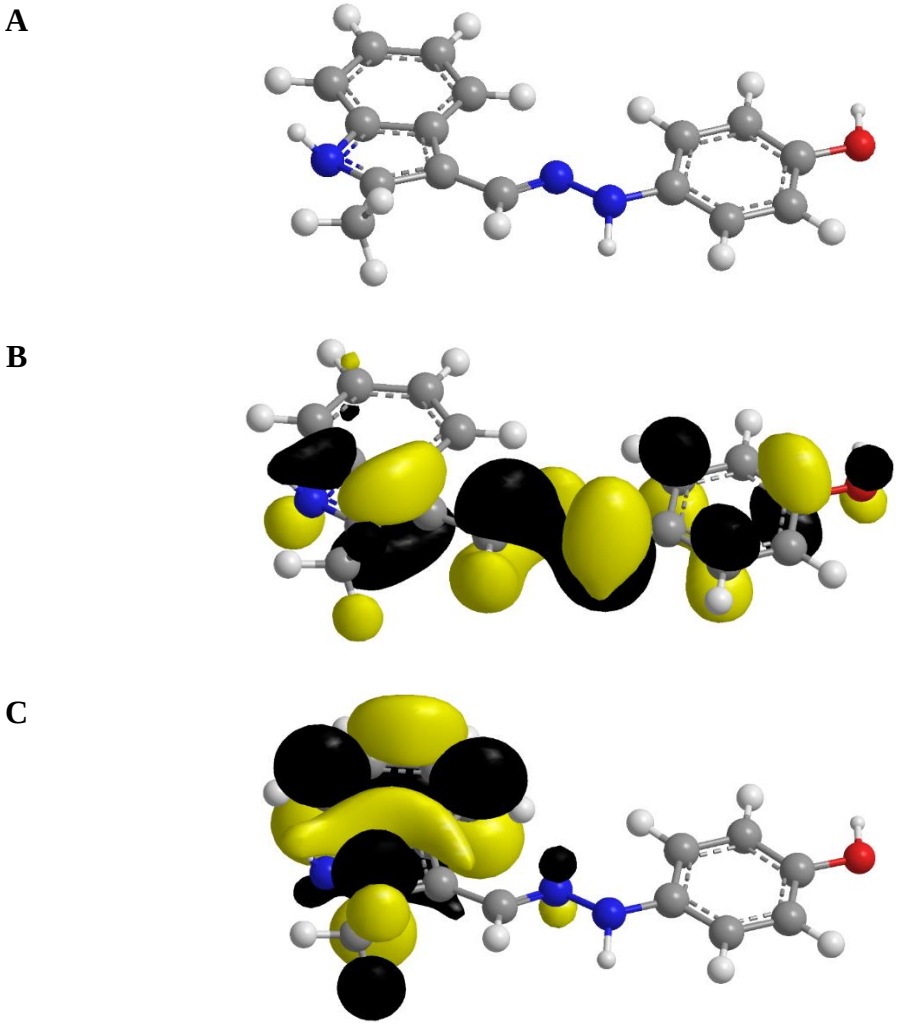

Figure 8. The (a) optimized structure, (b) highest occupied molecular orbital and (c) lowest unoccupied molecular orbital.

4. Conclusion

The results of the present study revealed that the (*E*)-4-(2-((2-methyl-1*H*-indol-3-yl)methylene)hydrazinyl)phenol, functioned as a good corrosion inhibitor for MS in 0.5 M HCl solution in a concentration-dependent mode. *IE* of new corrosion inhibitor maximum inhibition efficiency was up to 75% at 0.5 mM inhibitor concentration, our research unearthed several crucial insights, shaping the landscape of corrosion protection strategies:

1. Addressing mild steel's significance and corrosion vulnerability:

- Mild steel is a foundational material in a multitude of industrial applications, making its susceptibility to corrosion in acidic environments a paramount concern.
- The detrimental economic ramifications of corrosion underscore the imperative for innovative corrosion inhibitors to safeguard materials from degradation.

2. Corrosion inhibition properties:

- The synthesized inhibitor demonstrated exceptional efficacy in curbing mild steel corrosion. This was evident through significant reductions in corrosion rates and substantial enhancements in surface coverage.
- Polarization measurements revealed the inhibitor's capacity to modulate electrochemical kinetics by shifting the corrosion potential to more negative values and substantially reducing both anodic and cathodic current densities.

3. Insights into the mechanism of inhibition:

- The inhibition mechanism revolved around the adsorption of inhibitor molecules onto the mild steel surface.

4. Visual evidence of protection:

- Surface analysis through FESEM images provided compelling visual evidence of the inhibitor's effectiveness. It facilitated the formation of a protective layer on the mild steel surface, transforming the corroded morphology into a smoother, shielded state.

In conclusion, the synthesized compound has showcased promising corrosion inhibition properties, particularly for mild steel immersed in a challenging 0.5 M HCl medium. Its remarkable capacity to alter electrochemical kinetics, establish protective layers, and mitigate corrosive damage underscores its potential as an effective corrosion inhibitor. This study not only paves the way for novel corrosion protection strategies but also contributes to the sustainability and longevity of materials subjected to demanding industrial environments. Further research avenues may explore real-world applications and delve deeper into the intricate mechanisms governing its inhibitory behavior for a comprehensive understanding.

References

1. B.S. Mahdi, M.K. Abbass, M.K. Mohsin, W.K. Al-azzawi, M.M. Hanoon, M.H.H. Al-kaabi, L.M. Shaker, A.A. Al-amiery, W.N.R.W. Isahak, A.A.H. Kadhum and M.S. Takriff, Corrosion Inhibition of Mild Steel in Hydrochloric Acid Environment Using Terephthaldehyde Based on Schiff Base: Gravimetric, Thermodynamic, and Computational Studies, *Molecules*, 2022, **27**, no. 15, 4857. doi: 10.3390/molecules2715485726
2. A.M. Abdel-Gaber, H.T. Rahal and F.T. Beqai, Eucalyptus leaf extract as an eco-friendly corrosion inhibitor for mild steel in sulfuric and phosphoric acid solutions, *Int. J. Ind. Chem*., 2020, **11**, no. 2, 123–132. doi: 10.1007/s40090-020-00207-z
3. R.S. Al-Moghrabi, A.M. Abdel-Gaber and H.T. Rahal, Corrosion inhibition of mild steel in hydrochloric and nitric acid solutions using willow leaf extract, *Prot. Met. Phys. Chem. Surf*., 2019, **55**, 603–607. doi: 10.1134/S2070205119030031
4. H.T. Rahal, A.M. Abdel-Gaber and R. Awad, Influence of SnO_2 nanoparticles incorporation on the Electrochemical Behaviour of a Superconductor in Sodium Sulphate Solutions, *Int. J. Electrochem. Sci*., 2017, **12**, no. 11, 10115–10128. doi: 10.20964/2017.11.82
5. H.T. Rahal, A.M. Abdel-Gaber, R. Awad and B.A. Abdel-Naby, Influence of nitrogen immersion and NiO nanoparticles on the electrochemical behavior of (Bi, Pb)-2223 superconductor in sodium sulfate solution, *Anti-Corros. Methods Mater*., 2018, **65**, no. 4, 430–435. doi: 10.1108/ACMM-02-2018-1900
6. M.Y. El Sayed, A.M. Abdel-Gaber and H.T. Rahal, Safranin – a potential corrosion inhibitor for mild steel in acidic media: a combined experimental and theoretical approach, *J. Fail. Anal. Prev*., 2019, **19**, 1174–1180. doi: 10.1007/s11668-019-00719-6
7. W.K. Al-Azzawi, A.J. Al Adily, F.F. Sayyid, R.K. Al-Azzawi, M.H. Kzar, H.N. Jawoosh, A.A. Al-Amiery, A.A.H. Kadhum and M.S. Takriff, Evaluation of corrosion inhibition characteristics of an *N*-propionanilide derivative for mild steel in 1 M HCl: Gravimetrical and computational studies, *Int. J. Corros. Scale Inhib*., 2022, **11**, no. 3, 1100–1114. doi: 10.17675/2305-6894-2022-11-3-12
8. Y.M. Abdulsahib, A.J.M. Eltmimi, S.A. Alhabeeb, M.M. Hanoon, A.A. Al-Amiery, T. Allami and A.A.H. Kadhum, Experimental and theoretical investigations on the inhibition efficiency of *N*-(2,4-dihydroxytolueneylidene)-4-methylpyridin-2-amine for the corrosion of mild steel in hydrochloric acid, *Int. J. Corros. Scale Inhib*., 2021, **10**, no. 3, 885–899. doi: 10.17675/2305-6894-2021-10-3-3
9. A.K. Khudhair, A.M. Mustafa, M.M. Hanoon, A.Al-Amiery, L.M. Shaker, T. Gazz, A.H. Kadhum and M.S. Takriff, Experimental and theoretical investigation on the corrosion inhibitor potential of N-MEH for mild steel in HCl, *Prog. Color, Color. Coat*., 2022, **15**, no. 2, 111–122. doi: 10.30509/pccc.2021.166815.1111

10. D.S. Zinad, R.D. Salim, N. Betti, L.M. Shaker and A.A. Al-Amiery, Comparative investigations of the corrosion inhibition efficiency of a 1-phenyl-2-(1-phenylethylidene) hydrazine and its analog against mild steel corrosion in hydrochloric acid solution, *Prog. Color, Color. Coat.*,2022, **15**, no. 1, 53–63. doi: 10.30509/pccc.2021.166786.1108
11. R.D. Salim, N. Betti, M. Hanoon and A.A. Al-Amiery, 2-(2,4-Dimethoxybenzylidene)-*N*-phenylhydrazinecarbothioamide as an efficient corrosion inhibitor for mild steel in acidic environment, *Prog. Color, Color. Coat.*,2022, **15**, no. 1, 45–52. doi: 10.30509/pccc.2021.166775.1105
12. A.A. Al-Amiery, L.M. Shaker, A.H. Kadhum and M.S. Takriff, Exploration of furan derivative for application as corrosion inhibitor for mild steel in hydrochloric acid solution: Effect of immersion time and temperature on efficiency, *Mater. Today Proc*., 2021, **42**, 2968–2973. doi: 10.1016/j.matpr.2020.12.807
13. A.M. Resen, M.M. Hanoon, W.K. Alani, A. Kadhim, A.A. Mohammed, T.S. Gaaz, A.A.H. Kadhum, A.A. Al-Amiery and M.S. Takriff, Exploration of 8-piperazine-1-ylmethylumbelliferone for application as a corrosion inhibitor for mild steel in hydrochloric acid solution, *Int. J. Corros. Scale Inhib*., 2021, **10**, no. 1, 368–387. doi: 10.17675/2305-6894-2021-10-1-21
14. M.M. Hanoon, A.M. Resen, A.A. Al-Amiery, A.A.H. Kadhum and M.S. Takriff, Theoretical and experimental studies on the corrosion inhibition potentials of 2-((6-Methyl-2-Ketoquinolin-3-yl)Methylene)hydrazinecarbothioamide for mild steel in 1 M HCl, *Prog. Color. Color. Coat.*, 2022, **15**, no. 1, 11–23. doi: 10.30509/pccc.2020.166739.1095
15. F.G. Hashim, T.A. Salman, S.B. Al-Baghdadi, T. Gaaz and A. Al-Amiery, Inhibition effect of hydrazine-derived coumarin on a mild steel surface in hydrochloric acid, *Tribol. J. Tribol*., 2020, **37**, no. 3−4, 45–53. doi: 10.30678/fjt.95510
16. H.H. Ibraheem, A.S. Shubrem, Y.K. Al-Majedy and A.A. Issa, Experimental studies on the corrosion inhibition performance of chalcone derivative for mild steel in acid and alkaline solution, *AIP Conf. Proc*., 2022, **2443**, 030044. doi: 10.1063/5.0091889
17. A.A. Issa and H.R. Obayes, Capture carcinogenic aromatic compounds by the design of new tweezer compounds: a theoretical study, *J. Mol. Model*., 2020, **26**, no. 10, 292. doi: 10.1007/s00894-020-04558-3
18. Y.K. Al-Majedy, H.H. Ibraheem and A.A. Issa, Antioxidant, antimicrobial activity and quantum chemical studies of 4-methyl-7-hyroxy coumarin derivatives, *AIP Conf. Proc*., 2023, **2593**, 060002. doi: 10.1063/5.0113038
19. A.A. Alamiery, Investigations on corrosion inhibitory effect of newly quinoline derivative on mild steel in HCl solution complemented with antibacterial studies, *Biointerface Res. Appl. Chem*., 2022, **12**, no. 2, 1561–1568. doi: 10.33263/BRIAC122.15611568

20. I.A.A. Aziz, I.A. Annon, M.H. Abdulkareem, M.M. Hanoon, M.H. Alkaabi, L.M. Shaker, A.A. Alamiery, W.N.R.W. Isahak and M.S. Takriff, Insights into corrosion inhibition behavior of a 5-mercapto-1,2,4-triazole derivative for mild steel in hydrochloric acid solution: experimental and DFT studies, *Lubricants*,2021, **9**, no. 12, 122. doi: 10.3390/lubricants9120122
21. A. Alamiery, Short report of mild steel corrosion in 0.5 M H_2SO_4 by 4-ethyl-1-(4-oxo-4-phenylbutanoyl)thiosemicarbazide, *J. Tribol*., 2021, **30**, 90–99.
22. A.A. Alamiery, W.N.R.W. Isahak and M.S. Takriff, Inhibition of mild steel corrosion by 4-benzyl-1-(4-oxo-4-phenylbutanoyl)thiosemicarbazide: Gravimetrical, adsorption and theoretical studies, *Lubricants*, 2021, **9**, no. 9, 93. doi: 10.3390/lubricants9090093
23. A.A. Issa, H.H. Ibraheem and D.S. El Sayed, Computational innovation of in situ metallic elements with zirconia as a novel possible carrier for chemotherapeutic medication, *J. Mol. Model*., 2023, 30, no. 1, 14. doi: 10.1007/s00894-023-05815-x
24. M.A. Dawood, Z.M.K. Alasady, M.S. Abdulazeez, D.S. Ahmed, G.M. Sulaiman, A.A.H. Kadhum, L.M. Shaker and A.A. Alamiery, The corrosion inhibition effect of a pyridine derivative for low carbon steel in 1 M HCl medium: Complemented with antibacterial studies, *Int. J. Corros. Scale Inhib*., 2021, **10**, no. 4, 1766–1782. doi: 10.17675/2305-6894-2021-10-4-25
25. A. Alamiery, Corrosion inhibition effect of 2-*N*-phenylamino-5-(3-phenyl-3-oxo-1-propyl)-1,3,4-oxadiazole on mild steel in 1 M hydrochloric acid medium: Insight from gravimetric and DFT investigations, *Mater. Sci. Energy Technol*., 2021, **4**, 398–406. doi: 10.1016/j.mset.2021.09.002
26. A.A. Alamiery, Anticorrosion effect of thiosemicarbazide derivative on mild steel in 1 M hydrochloric acid and 0.5 M sulfuric Acid: Gravimetrical and theoretical studies, *Mater. Sci. Energy Technol*., 2021, **4**, 263–273. doi: 10.1016/j.mset.2021.07.004
27. A.A. Alamiery, WN.R.W. Isahak, H.S.S. Aljibori, H.A. Al-Asadi and A.A.H. Kadhum, Effect of the structure, immersion time and temperature on the corrosion inhibition of 4-pyrrol-1-yl-N-(2,5-dimethyl-pyrrol-1-yl)benzoylamine in 1.0 M HCl solution, *Int. J. Corros. Scale Inhib*., 2021, **10**, no. 2, 700–713. doi: 10.17675/2305-6894-2021-10-2-14
28. A. Alamiery, E. Mahmoudi and T. Allami, Corrosion inhibition of low-carbon steel in hydrochloric acid environment using a Schiff base derived from pyrrole: gravimetric and computational studies, *Int. J. Corros. Scale Inhib*., 2021, **10**, no. 2, 749–765. doi: 10.17675/2305-6894-2021-10-2-17
29. A.J.M. Eltmimi, A. Alamiery, A.J. Allami, R.M. Yusop, A.H. Kadhum and T. Allami, Inhibitive effects of a novel efficient Schiff base on mild steel in hydrochloric acid environment, *Int. J. Corros. Scale Inhib*., 2021, **10**, no. 2, 634–648. doi: 10.17675/2305-6894-2021-10-2-10
30. A. Döner, R. Solmaz, M. Özcan and G. Kardaş, Experimental and theoretical studies of thiazoles as corrosion inhibitors for mild steel in sulphuric acid solution, *Corros. Sci*., 2011, **53**, no. 9, 2902–2913. doi: 10.1016/j.corsci.2011.05.027

31. M.S. Abdulazeez, Z.S. Abdullahe, M.A. Dawood, Z.K. Handel, R.I. Mahmood, S. Osamah, A.H. Kadhum, L.M. Shaker and A.A. Al-Amiery, Corrosion inhibition of low carbon steel in HCl medium using a thiadiazole derivative: weight loss, DFT studies and antibacterial studies, *Int. J. Corros. Scale Inhib*., 2021, **10**, no. 4, 1812–1828. doi: 10.17675/2305-6894-2021-10-4-27
32. A.Z. Salman, Q.A. Jawad, K.S. Ridah, L.M. Shaker and A.A. Al-Amiery, Selected bis-thiadiazole: synthesis and corrosion inhibition studies on mild steel in HCl environment, *Surf. Rev. Lett*., 2020, **27**, no. 12, 2050014. doi: 10.1142/S0218625X20500146
33. S.B. Al-Bghdadi, M.M. Hanoon, J.F. Odah, L.M. Shaker and A.A. Al-Amiery, Benzylidene as efficient corrosion inhibition of mild steel in acidic solution, *Multidiscip. Digit. Publ. Inst. Proc*., 2019, **41**, no. 1, 27. doi: 10.3390/ecsoc-23-06472
34. B.S. Mahdi, H.S.S. Aljibori, M.K. Abbass, W.K. Al-Azzawi, A.H. Kadhum, M.M. Hanoon, W.N.R.W. Isahak, A.A. Al-Amiery and H.Sh. Majdi, Gravimetric analysis and quantum chemical assessment of 4-aminoantipyrine derivatives as corrosion inhibitors, *Int. J. Corros. Scale Inhib*., 2022, **11**, no. 3, 1191–1213. doi: 10.17675/2305-6894-2022-11-3-17
35. B. Hadi and H. Ibraheem, Synthesis, Characterization and Corrosion Inhibition of Novel Pyridine on Mild Steel in Hydrochloric Acid Environment, *J. Appl. Sci. Nanotechnol*., 2022, **2**, no. 2, 55–63. doi: 10.53293/jasn.3862.1050
.36 A.A. Alamiery, Study of corrosion behavior of *N′*-(2-(2-oxomethylpyrrol-1-yl)ethyl)piperidine for mild steel in the acid environment, *Biointerface Res. Appl. Chem*., 2022, **12**, no. 3, 3638–3646. doi: 10.33263/BRIAC123.36383646
37. Y. Al-Majedy and S. Shakir, Synthesis, Bio-evaluation and Quantum Chemical Studies of Some Coumarin Derivatives, *J. Appl. Sci. Nanotechnol*., 2021, **2**, no. 1, 20–27, doi: 10.53293/jasn.2021.4164.1076
38. A. Alamiery, A.B. Mohamad, A.A.H. Kadhum and M.S. Takriff, Comparative data on corrosion protection of mild steel in HCl using two new thiazoles, *Data Brief*., 2022, **40**, 107838. doi: 10.1016/j.dib.2022.107838
39. H.R. Obayes, G.H. Alwan, A.H.M.J. Alobaidy, A.A. Al-Amiery, A.A.H. Kadhum and A.B. Mohamad, Quantum chemical assessment of benzimidazole derivatives as corrosion inhibitors, *Chem. Cent. J*., 2014, **8**, 21. doi: 10.1186/1752-153X-8-21
40. S.B. Al-Baghdadi, F.G. Hashim, A.Q. Salam, T.K. Abed, T.S. Gaaz, A.A. Al-Amiery, A.A.H. Kadhum and K.S. Reda, Synthesis and corrosion inhibition application of NATN on mild steel surface in acidic media complemented with DFT studies, *Results Phys*., 2018, **8**, 1178–1184. doi: 10.1016/j.rinp.2018.02.007
41. A.M. Mustafa, F.F. Sayyid, N. Betti, M.M. Hanoon, A. Al-Amiery, A.A.H. Kadhum and M.S. Takriff, Inhibition Evaluation of 5-(4-(1*H*-pyrrol-1-yl)phenyl)-2-mercapto-1,3,4-oxadiazole for the Corrosion of Mild Steel in an Acidic Environment: Thermodynamic and DFT Aspects, *Tribol. J. Tribol*., 2021, 38, no. 3−4, 39–47. doi: 10.30678/fjt.105330

42. Y.K. Al-Majedy, H.H. Ibraheem, A.A. Issa and A. Alamiery, Exploring chromone derivatives as environmentally friendly corrosion inhibitors for mild steel in acidic environments: A comprehensive experimental and DFT study, *Int. J. Corros. Scale Inhib*., 2023, **12**, no. 3, 1028–1051. doi: 10.17675/2305-6894-2023-12-3-14
43. S. Al-Baghdadi, T.S. Gaaz, A. Al-Adili, A.A. Al-Amiery and M.S. Takriff, Experimental studies on corrosion inhibition performance of acetylthiophene thiosemicarbazone for mild steel in HCl complemented with DFT investigation, *Int. J. Low-Carbon Technol*., 2021, **16**, no. 1, 181–188. doi: 10.1093/ijlct/ctaa050
44. A.M. Mustafa, F.F. Sayyid, N. Betti, L.M. Shaker, M.M. Hanoon, A.A. Alamiery, A.A.H. Kadhum and M.S. Takriff, Inhibition of mild steel corrosion in hydrochloric acid environment by 1-amino-2-mercapto-5-(4-(pyrrol-1-yl)phenyl)-1,3,4-triazole, *South African J. Chem. Eng*., 2022, **39**, no. 1, 42–51. doi: 10.1016/j.sajce.2021.11.009
45. W.K. Al-Azzawi, S.M. Salih, A.F. Hamood, R.K. Al-Azzawi, M.H. Kzar, H.N. Jawoosh, L.M. Shakier, A. Al-Amiery, A.A.H. Kadhum, W.N.R.W. Isahak and M.S. Takriff, Adsorption and theoretical investigations of a Schiff base for corrosion inhibition of mild steel in an acidic environment, *Int. J. Corros. Scale Inhib*., 2022, **11**, no. 3, 1063–1082. doi: 10.17675/2305-6894-2022-11-3-10
46. D. Mahmood, A.K. Al-Okbi, M.M. Hanon, K.S. Rida, A.F. Alkaim, A.A.H. Al-Amiery, A. Kadhum and A.A.H. Kadhum, Carbethoxythiazole corrosion inhibitor: As an experimentally model and DFT theory, *J. Eng. Appl. Sci*., 2018, **13**, no. 11, 3952–3959. doi: 10.3923/jeasci.2018.3952.3959
47. A.H. Alobaidy, A. Kadhum, S.B. Al-Baghdadi, A.A. Al-Amiery, A.A.H. Kadhum, E. Yousif and A.B. Mohamad, Eco-friendly corrosion inhibitor: experimental studies on the corrosion inhibition performance of creatinine for mild steel in HCl complemented with quantum chemical calculations, *Int. J. Electrochem. Sci*., 2015, **10**, no. 5, 3961–3972. doi: 10.1016/S1452-3981(23)06594-X
48. A. Al-Amiery, L.M. Shaker, A.A.H. Kadhum, and M.S. Takriff, Synthesis, characterization and gravimetric studies of novel triazole-based compound, *Int. J. Low-Carbon Technol*., 2020, **15**, no. 2, 164–170. doi: 10.1093/ijlct/ctz067
49. S. Junaedi, A.A.H. Kadhum, A.A. Al-Amiery, A.B. Mohamad and M.S. Takriff, Synthesis and characterization of novel corrosion inhibitor derived from oleic acid: 2-Amino 5-Oleyl-1,3,4-Thiadiazol (AOT), *Int. J. Electrochem. Sci*., 2012, **7**, no. 4, 3543–3554. doi: 10.1016/S1452-3981(23)13976-9
50. H. Ibraheem, Y. Al-Majedy and A. Al-Amiery, 4-Thiadiazole: The biological activities, *Syst. Rev. Pharm*., 2018, **9**, no. 1, 36–40. doi: 10.5530/srp.2018.1.7
51. S.Sh. Batros, M.H. Ali and A.J. Addie, Microstructure-Modulated Antibacterial Performance of Chemically Precipitated SnO_2 Nanoparticles, *J. Appl. Sci. Nanotechnol*., 2023, **3**, no. 4, 20–32. doi: 10.53293/jasn.2023.7107.1246

♦ ♦ ♦